2019

# Nanosheets-in-nanotube Co3O4-carbon array design enables stable Li-ion storage

Dayi Guo
*Inner Mongolia University of Technology*

Lu Pan
*Beijing Jiaotong University*

Jianmin Hao
*Inner Mongolia University of Technology*

Limin Han
*Inner Mongolia University of Technology*

Ding Yi
*Beijing Jiaotong University*

***See next page for additional authors***

## Publication Details

Guo, D., Pan, L., Hao, J., Han, L., Yi, D., Wang, Y., Yang, Y., Bando, Y. & Wang, X. (2019). Nanosheets-in-nanotube Co3O4-carbon array design enables stable Li-ion storage. Carbon, 147 501-509.

# Nanosheets-in-nanotube Co3O4-carbon array design enables stable Li-ion storage

**Abstract**
Carbon composite products with different structures have been developed and used as anode for lithium-ion batteries due to the superior elasticity of carbon, which can keep the morphology integrity of the electrode materials in the process of the multiple cycles. Herein, a novel structure of nanosheets-in-nanotube Co 3 O 4 /carbon arrays is fabricated by the method of modified chemical vapor deposition (CVD). The carbon nanotube (CNT) layer acting as an outside coater can efficiently prevent the electrode from fragmentation and consequently ensure its shape integrity. The specific structure shows the ultra-stable cycle life (850 mAh g −1 after 200 cycles at 0.5C) and high rate capability (694 mAh g −1 at 2C). The favorable electrochemical properties are contributed to the combination of the wrapped elastic carbon and the enclosed Co 3 O 4 nanosheets in the lithiation process, which is confirmed by an in situ transmission electron microscope.

**Disciplines**
Engineering | Physical Sciences and Mathematics

**Publication Details**
Guo, D., Pan, L., Hao, J., Han, L., Yi, D., Wang, Y., Yang, Y., Bando, Y. & Wang, X. (2019). Nanosheets-in-nanotube Co3O4-carbon array design enables stable Li-ion storage. Carbon, 147 501-509.

**Authors**
Dayi Guo, Lu Pan, Jianmin Hao, Limin Han, Ding Yi, Yajing Wang, Yijun Yang, Yoshio Bando, and Xi Wang

# Nanosheets-in-nanotube $Co_3O_4$-carbon array design enables stable Li-ion storage

Dayi Guo [a, #], Lu Pan [b, c, #], Jianmin Hao [a, *], Limin Han [a], Ding Yi [b, c, **], Yajing Wang [c], Yijun Yang [b, c], Bando Yoshio [d, e, f], Xi Wang [b, c ,d]

[a] *College of Chemical Engineering, Inner Mongolia University of Technology, Hohhot 010051, P. R. China.*

[b] *Chemical and Chemical Engineering Guangdong Laboratory, Shantou, Guangdong, 5151031, P. R. China.*

[c] *Key Laboratory of Luminescence and Optical Information, Ministry of Education, Department of Physics, School of Science, Beijing Jiaotong University, Beijing, 100044, P. R. China.*

[d] *Tianjin Key Laboratory of Molecular Optoelectronic Sciences, School of Chemical Engineering and Technology, Tianjin University, Collaborative Innovation Center of Chemical Science and Engineering (Tianjin), Tianjin 300072, P. R. China.*

[e] *Australian Institute for Innovative Materials (AIIM), University of Wollongong, Squires Way, North Wollongong, NSW 2500, Australia.*

[f] *International Center for Young Scientists (ICYS), International Center for Materials Nanoarchitectonics (MANA), National Institute for Materials Science (NIMS), Namiki 1-1, Tsukuba, Ibaraki 305-0044, Japan.*

**Abstract**

Carbon composite products with different structures have been developed and used as anode for lithium-ion batteries due to the superior elasticity of carbon, which can keep the morphology integrity of the electrode materials in the process of the multiple cycles. Herein, a novel structure of nanosheets-in-nanotube $Co_3O_4$/carbon array is fabricated by the method of modified chemical vapor deposition. The carbon nanotube

layer acting as an outside coater can efficiently prevent the electrode from fragmentation and consequently ensure its shape integrity. The specific structure shows the ultra-stable cycle life (850 mAh $g^{-1}$ after 200 cycles at 0.5C) and high rate capability (694 mAh $g^{-1}$ at 2C). The favorable electrochemical properties are contributed to the combination of the wrapped elastic carbon and the enclosed $Co_3O_4$ nanosheets in the lithiation process, which is confirmed by an *in situ* transmission electron microscope.

* Corresponding author.

** Corresponding author.

E-mail addresses: haojmin@foxmail.com (Jianmin Hao), yiding15@gmail.com (Ding Yi)

## 1. Introduction

Lithium-ion batteries (LIBs) have been widely used in many aspects as one of most promising secondary batteries because of their environmental friendliness, fast charge/discharge ability, high power density and long cycle life [1-4]. As the most commercially applied anode materials, graphite belongs to the single-electron type with the maximum theoretical capacity of 372 mAh $g^{-1}$ ($LiC_6$). In order to meet the increasing demand of the energy storage devices, the multi-electrons-materials are believed as the next-generation anode candidates for LIBs. Among them, the conversion-mechanism-based ones including metal oxides [5-8] and metal sulfides [9,10] were believed to be promising ones, due to their high capacity (about 2-2.5 times higher than commercial graphite). However, these classes of materials suffered from huge volume changes during charging-discharging process, leading to the pulverization of the electrode and thus the severe capacity fading [11-14]. To solve such a problem, the carbon composite products with different structures were prepared by many researchers, because carbon exhibits the superior elasticity theoretically, which can keep the morphology integrity of the electrode materials in the process of the multiple cycles. For instance, Ding *et al*. have made uniform core-shell Co@C microspheres through the *in situ* transformation from $Co_3O_4$@phenolic [15]; $Co_3O_4$/Co@N-doped carbon nanotubes have been fabricated by Chen's group with improving cycling stability [16]; Deng *et al.* made three-dimensionally hierarchical $Co_3O_4$/Carbon composites with excellent electrochemical performances [17]. In despite of the big processes made in this area [18], there are few reports on the structure of an array consisted of two-dimensional nanosheets-in-carbon nanotubes. Theoretically, such a novel structure's stability towards $Li^+$ storage is dramatically improved, and thus the electrochemical performance will be greatly promoted. Whereas, it is a great challenge

to synthesize this type of structure.

Herein, we fabricated such a new ideal structure of nanosheets-in-nanotube $Co_3O_4$/carbon arrays (NIN arrays) by utilizing a modified chemical vapor deposition method. This structure exhibited much improved cycling stability when tested as anodes in LIBs. We also used an *in situ* transmission electron microscopy (*in situ* TEM) [19] to observe the lithiation process of as-designed anode in real time, suggesting that the carbon layer acting as an outside coater could efficiently prevent the electrode from fragmentation and consequently ensure the shape integrity of the electrode. Furthermore, the unique array feature could enable a fast $Li^+$ transportation, and the inner ultrathin $Co_3O_4$ nanosheets (NSs) are beneficial to improve the electrochemical performance due to their specific two-dimensional structure [20,21]. Above-mentioned structural characteristics of an NIN will make it show the superior cycling stability and a high rate capability.

## 2. Experimental Section

### 2.1 Synthesis of NIN arrays

The structure of NIN arrays was fabricated by the following steps. Firstly, the method of chemical vapor deposition (CVD) was used to synthesis carbon nanotube (CNT) arrays. The specific operation was to put the anodic aluminium oxide (AAO) template (with a thin layer of Cu on the one side which can prevent the structures from collapsing after removing the templates) and liquid paraffin into the tube furnace and heat to 850ºC in argon flow (100 sccm) for 1 h, then cool the furnace to room temperature in argon flow sequentially. Secondly, with a reaction ion etching system (L-451D-L, ANELVA), the prepared AAO@carbon was plasma etched for 1 h (Ar buffer gas, 100 W, 5 Pa) to eliminate the amorphous carbon layer which shaped by the chemical vapor deposition. Thirdly, the acquired AAO@carbon and 0.1 mol $Co(NO_3)_2$ was added into the aqueous

alkali (PH=9), then the mixed solution was put into reaction kettle and heated to 170ºC for 12 h. After reaction, with the operation of filtration as well as rinse by DI water and alcohol, the obtained solid-state material was dried in an oven at 350ºC for 2 h under the atmosphere of nitrogen. Ultimately, the $Co_3O_4$ nanosheets (NSs) which presented as black powder were successfully grown in the interior surface of the CNTs. In the final step of the process, the sample of NIN arrays was put into 3 M NaOH solution for 1 h to dissolving the AAO template. After the thoroughly rinsing and drying procedure, the structure of nanosheets-in-nanotube $Co_3O_4$/carbon array was obtained.

**2.2 Characterization**

Scanning electron microscopy (SEM, Hitachi S-4800, operated at 10 kV), transmission electron microscopy (TEM, JEOL JEM-2100F, with an accelerating voltage of 300 kV), fast Fourier transform (FFT) and high-angle annular dark-field (HAADF) scanning transmission electron microscopy (STEM, JEOL JEM-2100F) were used to characterize the morphology of the $Co_3O_4$/carbon array. X-ray diffraction (XRD, Philips X'Pert PRO MPD X-ray diffractometer, operated at 35 kV and 45 mA with Cu Kα radiation) and energy dispersive spectrometer (EDS, JEOL JEM-2100F) element mapping were used to investigate the crystal phase, structure and chemical component of the samples. X-ray photoelectron spectroscopy (XPS) was used to characterize the element chemical states.

**2.3 Electrochemical measurements**

Three-electrode cells were used to measure the electrochemical properties of the NIN arrays and the Li metal foil was selected as the reference and counter electrode. There was 1 M $LiClO_4$ in ethyl carbonate (EC) and diethyl carbonate (DEC) (EC/DEC = 1/1 in v/v) which made up the electrolyte. Then the cells were assembled in a glove box which filled with pure argon gas. In a potential range of 3-0.05 V, the galvanostatic

discharge/charge measurements were performed vs $Li^+/Li$. The specific capacity of the NIN arrays was calculated based on the total weight of nanosheets-in-nanotube $Co_3O_4$/carbon array.

### 2.4 Construction of the NIN-based LIBs

*In situ* transmission electron microscopy observations were implemented in a JEOL JEM-2100F equipped with a Nanofactory Instruments STM-TEM holder. In order to build up the text cell, an individual NIN was attached to the gold rod, which was further attached to the piezo-manipulator. A small piece of lithium foil was also attached to another gold wire as a reference and counter electrode. An ionic liquid electrolyte (ILE) was prepared in advance by dispersion of lithium bis(trifluoromethylsulfonyl)imide (LiTFSI) into N-methyl-N-propylpiperidinium bis(trifluoromethanesulfonyl)imide (PP13TFSI). Before insertion of the holder into the TEM, a drop of the ILE was placed on the surface of metal lithium tip. It was easy to choose an isolated NIN. The lithiation was carried out at a negative bias in the range of -3-0 V with respect to the Li metal.

## 3. Results and discussion

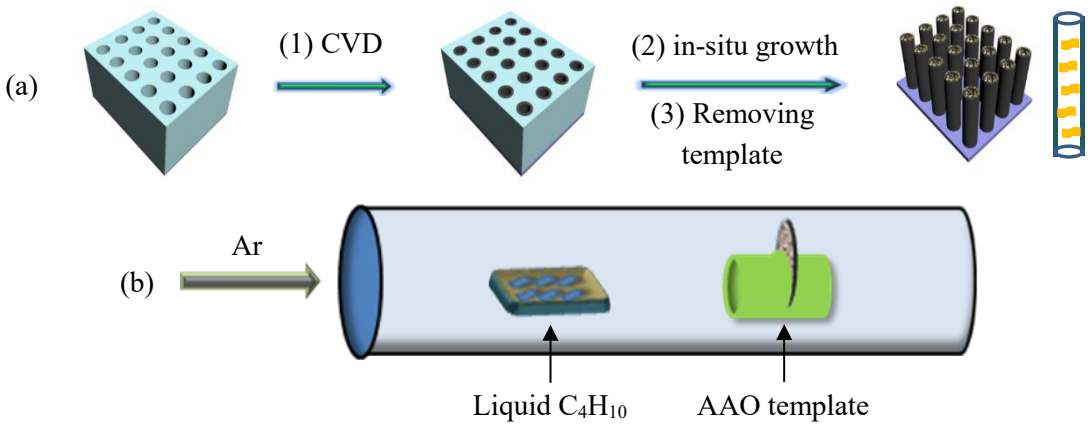


Fig. 1. (a) Schematic design and fabrication process of nanosheets-in-nanotube $Co_3O_4$/carbon arrays structure. (b) Schematic of the synthesis process of CNTs using the AAO template.

The synthetic procedure of the NIN arrays including three steps is shown in Fig. 1a. Firstly, the carbon nanotubes (CNTs) were grown into the anodic aluminium oxide (AAO) template. Herein, a modified CVD approach is used. As depicted by Fig. 1b, the AAO template was put into a specially made small quartz tube vertically in the middle of tube furnace and a porcelain boat loaded the $C_4H_{10}$ was placed at the gas intake side of the tube. The high temperature of 850ºC can guarantee the $C_4H_{10}$ transformation into carbon on surface of the AAO template. In consideration of the large surface area and well-distributed nanopores (Fig. S1a and S1b), AAO membranes have been widely applied to synthesize nanomaterials in the energy field [22]. The panorama of the AAO template presents its height of ~60 μm (Fig. S1c) and its cross-section show a smooth interior structure with the width of 200-400 nm (Fig. S1d). Secondly, $Co_3O_4$ NSs were planted into inner-walls of CNTs with the assistant of an *in situ* growth method (Fig. 1a). In this step, the existence of AAO@CNTs is of key importance to ensure totally forming $Co_3O_4$ NSs in CNTs instead of the outside walls of CNTs. It is worthy to note that the presence of the trace of oxygen in CNTs will be beneficial to fabricate $Co_3O_4$ NSs due to their hydrophilic surfaces. Therefore, the $Co_3O_4$ NSs was planted inside the CNTs. Finally, the designed nanosheets-in-nanotube $Co_3O_4$/carbon array (NIN arrays) structure was successfully obtained after removing the AAO template. As shown in Fig. 2a, the special structure of nanosheets-in-nanotube can be clearly observed by the vertical section view of the NIN arrays.

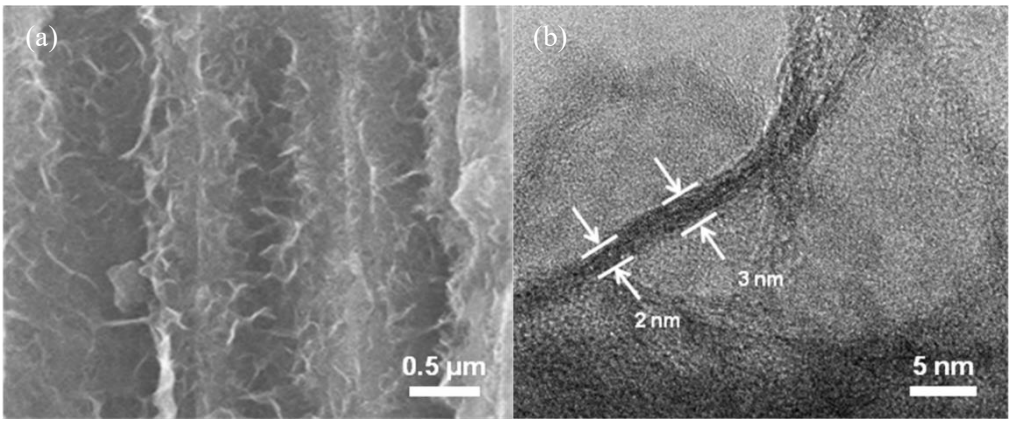


Fig. 2. (a) SEM image on the cross section of the broken nanosheets-in-nanotube $Co_3O_4$/carbon arrays structure. (b) HRTEM image of $Co_3O_4$ nanosheets from a side view.

The detailed structure and morphology of NIN arrays and the pure CNTs were investigated, proving that the as-designed structure has been fabricated successfully. The X-ray diffraction (XRD) pattern of NIN arrays is shown in Fig. 3a, the peaks in pattern can be indexed to the spinel $Co_3O_4$ (JCPDS no. 42-1467) which authenticates the existence of $Co_3O_4$. According to the SEM image in Fig. 3b, the configuration of nanotube arrays can be observed arranging in order on the copper film and the length of the CNTs is ~50 μm. TEM image at higher magnification (Fig. 3c) of an individual carbon nanotube clearly reveals the morphology of the fabricated structure: nanosheets-in-nanotube, confirming to the schematic depicted as the inset in Fig. 3c. As can be seen, the width of a single tube is ~200 nm, the thickness of CNTs is ~10 nm and the thickness of $Co_3O_4$ NSs is 2-3 nm (Fig. 2b). The high-resolution TEM image of $Co_3O_4$ NSs shown in Fig. 3d exhibits the lattice fringes for an interplanar spacing of 0.47 nm, corresponding to the (111) lattice exposed facet of $Co_3O_4$. The presented (111) facet is usually considered as a high-energy facet relatively, which can bring about more active sites for $Li^+$ storage, thus improving the electrochemical performance of the Lithium ion batteries [23]. The thermogravimetric curve of NIN arrays (Fig. S2) shows that a

weight loss of ~10% occurs in the temperature range from 300ºC to 375 ºC due to the loss of CNTs, which proves that the mass content of CNTs is ~10%.

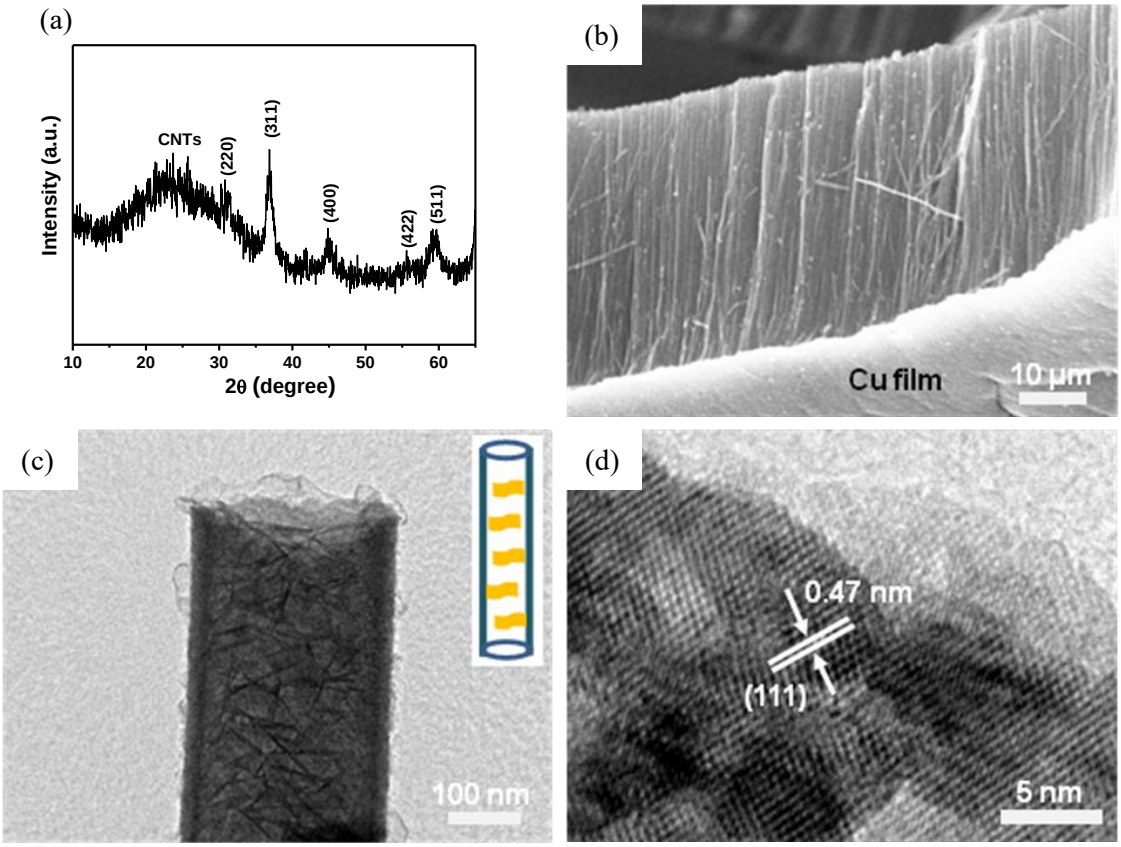


Fig. 3. (a) XRD pattern of nanosheets-in-nanotube $Co_3O_4$/carbon arrays on the Cu foil. (b) SEM characterizations of nanosheets-in-nanotube $Co_3O_4$/carbon arrays. (c) TEM image at higher magnification of an individual nanosheets-in-nanotube $Co_3O_4$/carbon array structure. Inset showing the schematic drawing of nanosheets-in-nanotube $Co_3O_4$/carbon array. (d) HRTEM images of a nanosheets-in-nanotube $Co_3O_4$/carbon array layer.

As a comparison, the pure CNTs were also made by the similar synthetic method (Fig. 4a). According to the XRD pattern in Fig. 4b, it is noted that there is a broad peak at about 22° which can be attributed to CNTs. Compared with the sharp peak of the pure CNTs, the contrasting result illustrates that the as-prepared sample is composed of both $Co_3O_4$ and carbon. SEM images of CNTs shows the structure of hollow tubes (Fig.

4c and 4d) with the size of ~200 nm wide and ~50 μm long which is accord with the size of NINs. The most remarkable feature of NIN arrays is growing the $Co_3O_4$ NSs in the interior wall of CNTs. The high-angle annular dark-field scanning transmission electron microscopy (HAADF STEM) and energy dispersive spectrometer (EDS) element mapping images of an NIN are also given as the direct evidence in Fig. 4. Compared with the image of pure CNTs (Fig. 4e) the image of NIN array (Fig. 4f) shows that the CNT is stuffed with $Co_3O_4$ NSs with smooth outer surface. It also can be obviously observed that signals of oxygen and cobalt are uniformly covered within the boundary (Fig. 4g and 4h), indicating that $Co_3O_4$ NSs are well introduced into CNTs. Meanwhile, the carbon signals (Fig. 4j) are distributed wider than oxygen and cobalt crossing the boundary, which means that the $Co_3O_4$ NSs are wrapped by CNTs completely. It is noted that there are only signals of carbon and a very small amount of oxygen in pure CNTs (Fig. 4e). It turns out to be the case that the $Co_3O_4$ NSs was completely planted inside the CNTs.

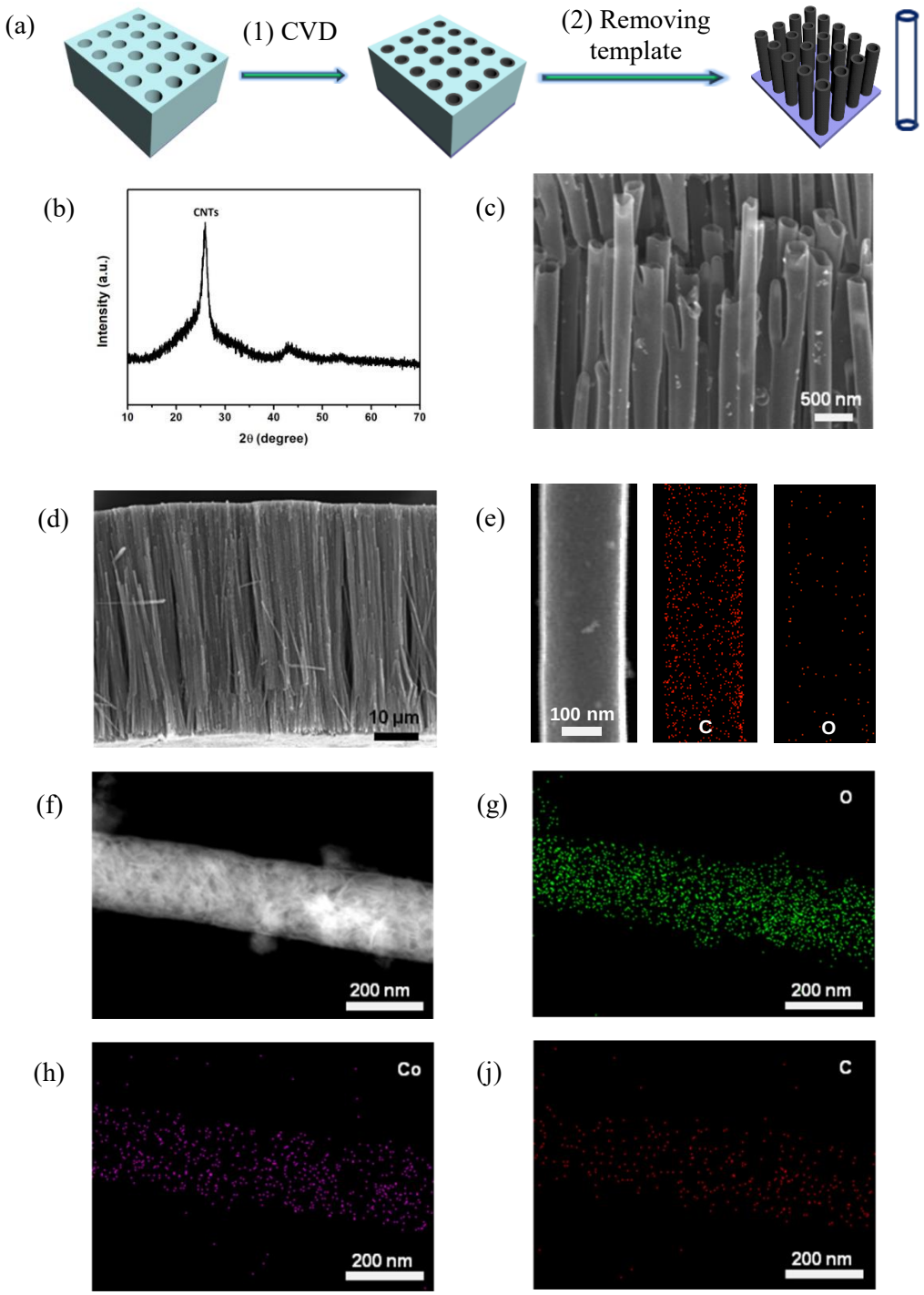


Fig. 4. (a) Schematic of the fabrication process of the pure carbon nanotubes. (b) XRD pattern of carbon nanotubes. (c, d) SEM characterizations of carbon nanotubes. (e) HAADF STEM image and the EDS element mappings of C and O of carbon nanotubes. (f) HAADF STEM image of the nanosheets-in-nanotube $Co_3O_4$/carbon arrays structure. The EDS element mappings of O (g), Co (h) and C (j) of the nanosheets-in-nanotube

$Co_3O_4$/carbon arrays structure.

Chemical states of cobalt states of the NIN arrays were carried out by XPS (Fig. 5). The spectra of NIN arrays exhibit two peaks at 778.8 eV and 795.7 eV while two satellite peaks at 783.9 eV and 801.4 eV, corresponding to the Co $2p_{3/2}$ and Co $2p_{1/2}$ spin-orbit peaks of $Co_3O_4$ respectively, which is identical with the foregoing analysis testifying the formation of $Co_3O_4$ phase. According all these characterizations above, the unique structure of nanosheets-in-nanotube can be generally verified.

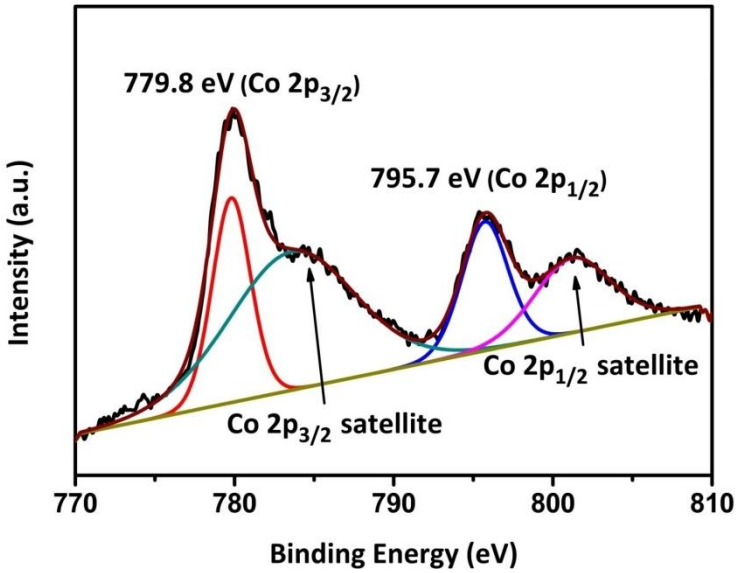


Fig. 5. High-resolution XPS spectra of nanosheets-in-nanotube $Co_3O_4$/carbon arrays.

The battery performance of NIN arrays was evaluated and compared with the commercial $Co_3O_4$ samples by galvanostatic charge/discharge measurement and electrochemical impedance spectroscopy (EIS) and the results are given in Fig. 6. Such NIN arrays indeed showed a superior and stable electrochemical performance. Fig. 6a shows the first galvanostatic charge/discharge cycle of NIN arrays under the current density of 0.2C (1C = 890 mAh $g^{-1}$). The potential plateau at 1.2 V is related to the conversion of $Co_3O_4$ into an intermediate phase CoO (or $Li_XCo_3O_4$), and then the metallic Co was formed, indicating a typical charge/discharge behavior of the $Co_3O_4$

electrode materials [24,25]. The initial charge and discharge capacities are 1189.3 mAh $g^{-1}$ and 1279.2 mAh $g^{-1}$, respectively. It is noted that there is a relatively high initial Coulombic efficiency of 92.9%. The irreversible capacity loss in first cycle may be caused by the irreversible reactions, electrolyte decomposition and the formation of SEI layer on the surface of electrode [20]. In Fig. 6b, the comparative cyclic performances of the NIN arrays and the commercial $Co_3O_4$ samples at a current density of 0.5C are exhibited. The NIN array delivers a specific capacity of 850 mAh $g^{-1}$ after 205 cycles with a Coulombic efficiency of 99.9%, exhibiting a superior cycling performance and good reversibility, while the capacity of commercial $Co_3O_4$ samples substantially decreases to only 157 mAh $g^{-1}$ after 50 cycles. The magnified Coulombic efficiency curve (Fig. S3) also shows the fluctuation, which is consistent with variation trend of the charge-discharge capacities. As demonstrated in Fig. 6c, rate capability of NIN arrays is evaluated at different current densities ranging from 0.2C to 2C. As is revealed, even at a high current density of 2C, the reversible capacity still remained around 694 mAh $g^{-1}$, which is 1.87 times higher than that of graphite (372 mAh $g^{-1}$). It demonstrates that such special structure could facilitate $Li^+$ ion transportation. In addition, the contrastive electrode kinetics of NIN arrays and commercial $Co_3O_4$ samples were analyzed by EIS in Fig. 6d, which conducted with 5 mV amplitude in the frequency range from 0.01 Hz to 100 kHz. On the high frequency region of the curves, the arc diameter of NIN arrays is smaller than that of commercial $Co_3O_4$, which means the charge transfer resistance of NIN arrays is lower. In intermediate frequency region, the included angle of spectral line and real axis of NIN arrays is close to 90° while the angle of commercial $Co_3O_4$ is about 45°. The high angle indicating that the diffusion velocity of ions to electrode is much faster. The diagonal in low frequency region is attributed to the Warbug impedance of ions on the electrode. The higher slope of NIN arrays

explains that it has a higher electrochemical capacity than that of the commercial $Co_3O_4$. Compared with the previously reported $Co_3O_4$ related anode materials for LIBs (Table 1), NIN anode exhibited relatively enhanced electrochemical performances, especially on the aspect of cycle life. The desirable properties of NIN arrays are attributed to its unique nanosheets-in-nanotube structure features.

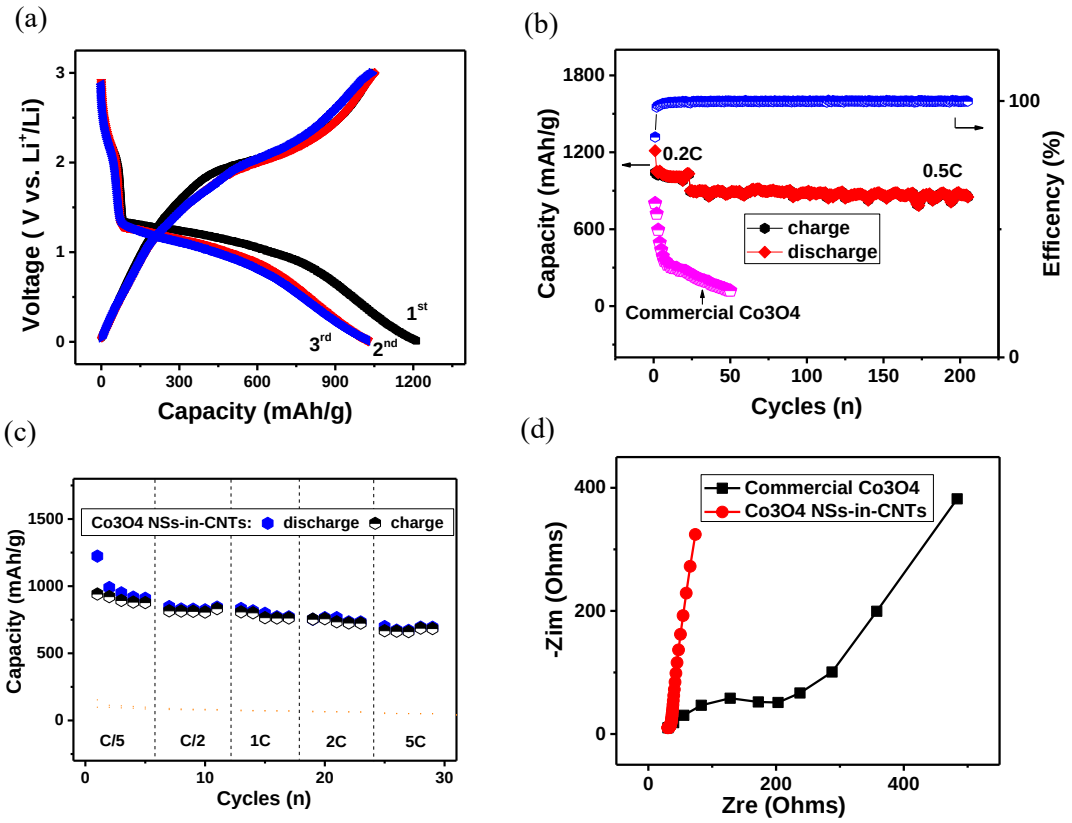


Fig. 6. Electrochemical lithium storage properties of nanosheets-in-nanotube $Co_3O_4$/carbon arrays: (a) Charge/discharge voltage profiles of nanosheets-in-nanotube $Co_3O_4$/carbon arrays at a current density of 0.2C. (b) Cycling performance and Coulombic efficiency of nanosheets-in-nanotube $Co_3O_4$/carbon arrays and commercial $Co_3O_4$ at a current density of 0.2C. (c) Rate performance of nanosheets-in-nanotube $Co_3O_4$/carbon arrays at different current density. (d) EIS of nanosheets-in-nanotube $Co_3O_4$/carbon arrays and commercial $Co_3O_4$.

Table 1 Comparisons on LIBs performance between different $Co_3O_4$-based anodes.

| Electrode materials | First discharge-charge capacity (mAh $g^{-1}$) | Cycling performance (mAh $g^{-1}$) | Ref. |
|---|---|---|---|
| $Co_3O_4$ NSs-in-CNT arrays | 1279-1189 at 178 mA $g^{-1}$ | 850 after 205 cycles at 445 mA $g^{-1}$ | This work |
| Peapod-like $Co_3O_4$@carbon nanotube | ~1250-~780 at 100 mA $g^{-1}$ | 700 after 100 cycles at 100 mA $g^{-1}$ | [26] |
| Porous MWCNTs/$Co_3O_4$ nanocomposites | 1171-812 at 100 mA $g^{-1}$ | 813 after 100 cycles at 100 mA $g^{-1}$ | [27] |
| Hollow-structured $Co_3O_4$ particles | 1107-~800 at 50 mA $g^{-1}$ | 880 after 50 cycles at 50 mA $g^{-1}$ | [28] |
| $Co_3O_4$/N-doped porous carbon | 1730-1321 at 100 mA $g^{-1}$ | 892 after 100 cycles at 100 mA $g^{-1}$ | [29] |
| $Co_3O_4$@a-$TiO_2$ core-shell microcubes | 1100-790 at 500 mA $g^{-1}$ | 800 after 60 cycles at 500 mA $g^{-1}$ | [30] |
| Mesoporous nanostructured $Co_3O_4$ | 1286-880 at 200 mA $g^{-1}$ | 913 after 60 cycles at 200 mA $g^{-1}$ | [31] |
| Co/$Co_3O_4$-C ternary core-branch arrays | 1195-880 at 445 mA $g^{-1}$ | 608 after 200 cycles at 445 mA $g^{-1}$ | [32] |
| $Co_3O_4$/MWNT composites | 960-670 at 100 mA $g^{-1}$ | 708 after 100 cycles at 100 mA $g^{-1}$ | [33] |
| Self-stacked $Co_3O_4$ nanosheets | 1644-~1050 at 178 mA $g^{-1}$ | 1070 after 50 cycles at 178 mA $g^{-1}$ | [34] |
| Double-shelled $Co_3O_4$ hollow spheres | 1013-~750 at 178 mA $g^{-1}$ | 866 after 50 cycles at 178 mA $g^{-1}$ | [35] |

The lithiation process of NIN array and its related storage mechanisms at the atomic level were unmasked via an *in situ* TEM [36]. An *in situ* battery prototype (the experimental part, ESI) was set up as illustrated in Fig. 7a. The structure is composed of a piece of NIN arrays, an ionic liquid electrolyte and a tablet of metallic Li. With a potential of -3 V between the metal Li electrode and NIN, the process of lithiation is brought to pass. The top-left inset in Fig. 7c is the fast Fourier transform (FFT) image that indicates the phase generation of $Li_2O$ and Co. Upon lithiation (Fig. 7b and 7c), NIN was slightly expanded. In order to facilitate a detailed observation of the volume change of NIN, the area framed up by red squares in Fig. 7b and Fig. 7c are magnified and shown in Fig. 7d and Fig. 7e. Although the relatively high amounts of $Co_3O_4$ NSs were filled into CNTs, there still exist some void spaces in the hollow shell of CNT including the interspaces came from the room sites (areas circled by the red line in Fig.

7d and 7e) and the interval void spaces resulting from the crisscross of $Co_3O_4$ NSs (Fig. S1a). Therefore, when the intercalation of $Li^+$ into $Co_3O_4$ NSs happens, these two kinds of hollow spaces can effectively buffer the volume expansion. Such a process is obviously visualized via an *in situ* TEM, as shown in Fig. 7d and 7e, after full lithiation, the void spaces still exist (Fig. 7e), which indicates that the elastic of CNT can effectively endure the expansion. Many theoretical studies at early time showed that the maximum elastic strain (fracture strain) of CNTs is about 18% [37-39], and the elastic strain of CNTs in this work is smaller by calculation (in Fig. 7d and Fig. 7e the diameter of CNTs increases from 200 nm to 210 nm; the formula of elastic strain is $\Delta d/d$), thus the whole structure will not be broken with the volume expansion. In addition, the volume expansion rate is 105% (200 nm to 210 nm) in the $Li^+$-insertion process, much smaller than that of the pure $Co_3O_4$. These findings demonstrate that the ultrahigh elastic property of CNT and the unique structure features can strength the structural stability of NIN. The phase and structure evolution of a single $Co_3O_4$ nanosheet was further observed. Before $Li^+$ intercalation, a nanosheet was a single crystal plate with a 0.47 nm lattice spacing (Fig. 7f), corresponding to (111) plane of $Co_3O_4$. After $Li^+$ intercalation, the $Co_3O_4$ NSs turned to the confused particles and their main composition was further proofed as the metal cobalt (Fig. 7g) (0.21 nm interplanar spacing is assigned to (100) facet of cobalt). It also agrees with the transformation process in the classic conversion mechanism: $Co_3O_4+Li \rightarrow Li_2O+Co$. Above all, the whole NIN structure is well preserved during $Li^+$ insertion, thus leading to superior cycling stability.

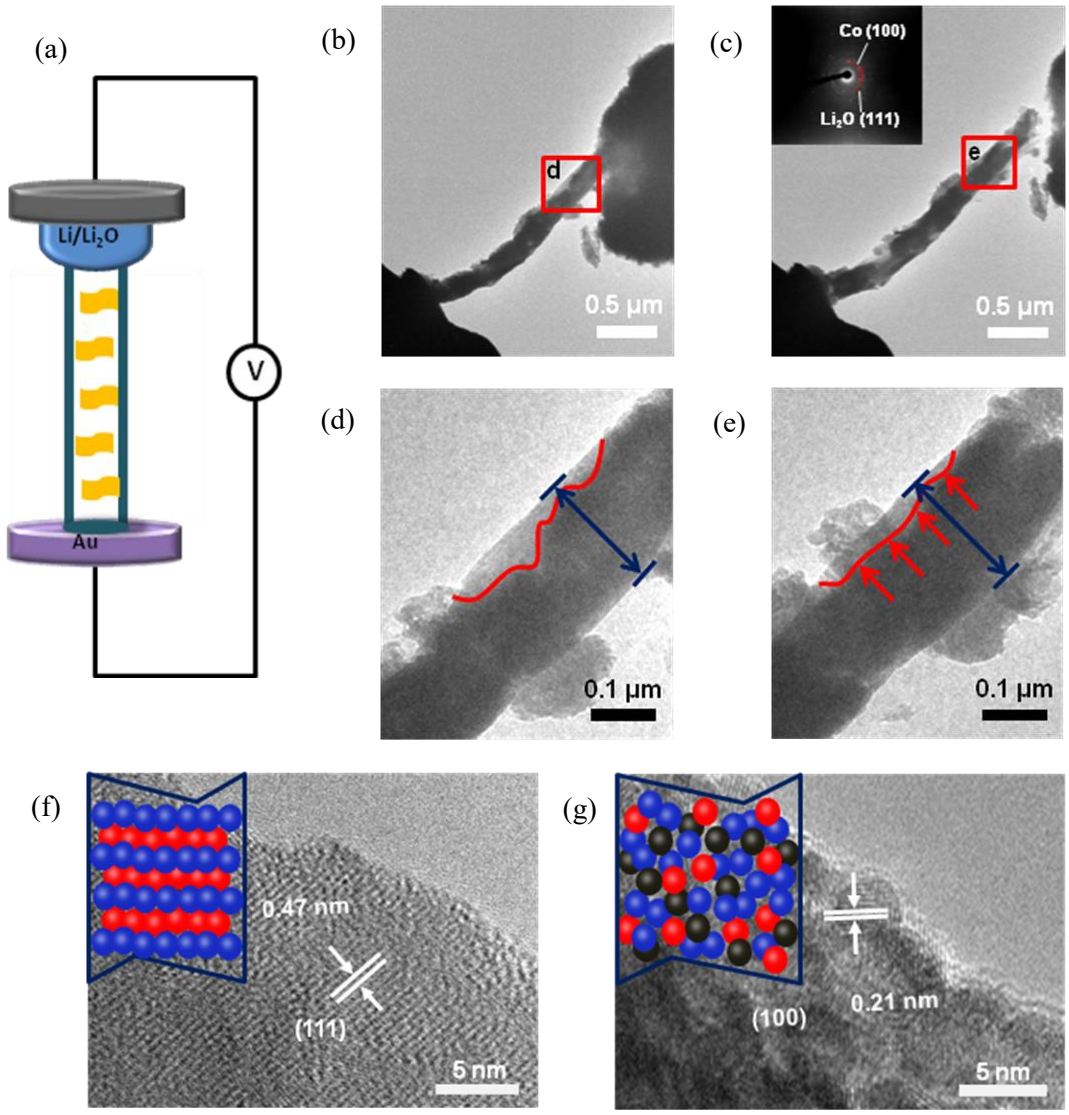


Fig. 7. (a) Schematic illustration of a LIB device with the anode of nanosheets-in-nanotube $Co_3O_4$/carbon arrays under *in situ* TEM. (b, c) *In situ* TEM patterns during Li ion intercalation and the FFT patterns of a nanosheets-in-nanotube $Co_3O_4$/carbon array. (d, e) TEM image at higher magnification of a nanosheets-in-nanotube $Co_3O_4$/carbon array. (f, g) HRTEM images of a nanosheets-in-nanotube $Co_3O_4$/carbon array layer before and after the Li ion intercalation. Inset showing the schematic drawing of the atomic structure.

The superior electrochemical performance of the stable structure of NIN arrays is considered to be attributed to its unique configuration. As shown in Fig. 8a, the outer

carbon layer can reinforce the whole structure as well as provide continuous conductive paths. It can protect the interior $Co_3O_4$ NSs from wastage during the volume expansion caused by the phase transition, promoting the cyclic performance and specific capacities of the architecture. Besides, the interspaces in this array structure can be easily filled with the electrolyte, which can enlarge the contacting area and enhance the $Li^+$ transport. Just as significant, the crystal plane of $Co_3O_4$ also plays an important role on its electrochemical performances. In our case, the (111) facts are highly exposed. Relatively, the (111) facets have more cobalt atoms on the surfaces of $Co_3O_4$ crystals which is 1.875 $Co^{2+}$ (Fig. 8b) while the (001) facets have 1 $Co^{2+}$ (Fig. 8c). From this point of view, NIN arrays with highly exposed (111) facets is good for improving their capacity of the structure. After cycling, the structure of nanotube is well preserved (Fig. S4a), indicating the stability of NIN arrays. The XRD pattern (Fig. S4b) exhibits a broad Co peak, suggesting the existence of ultra-small Co nanoparticles dispersed in $Li_2O$.

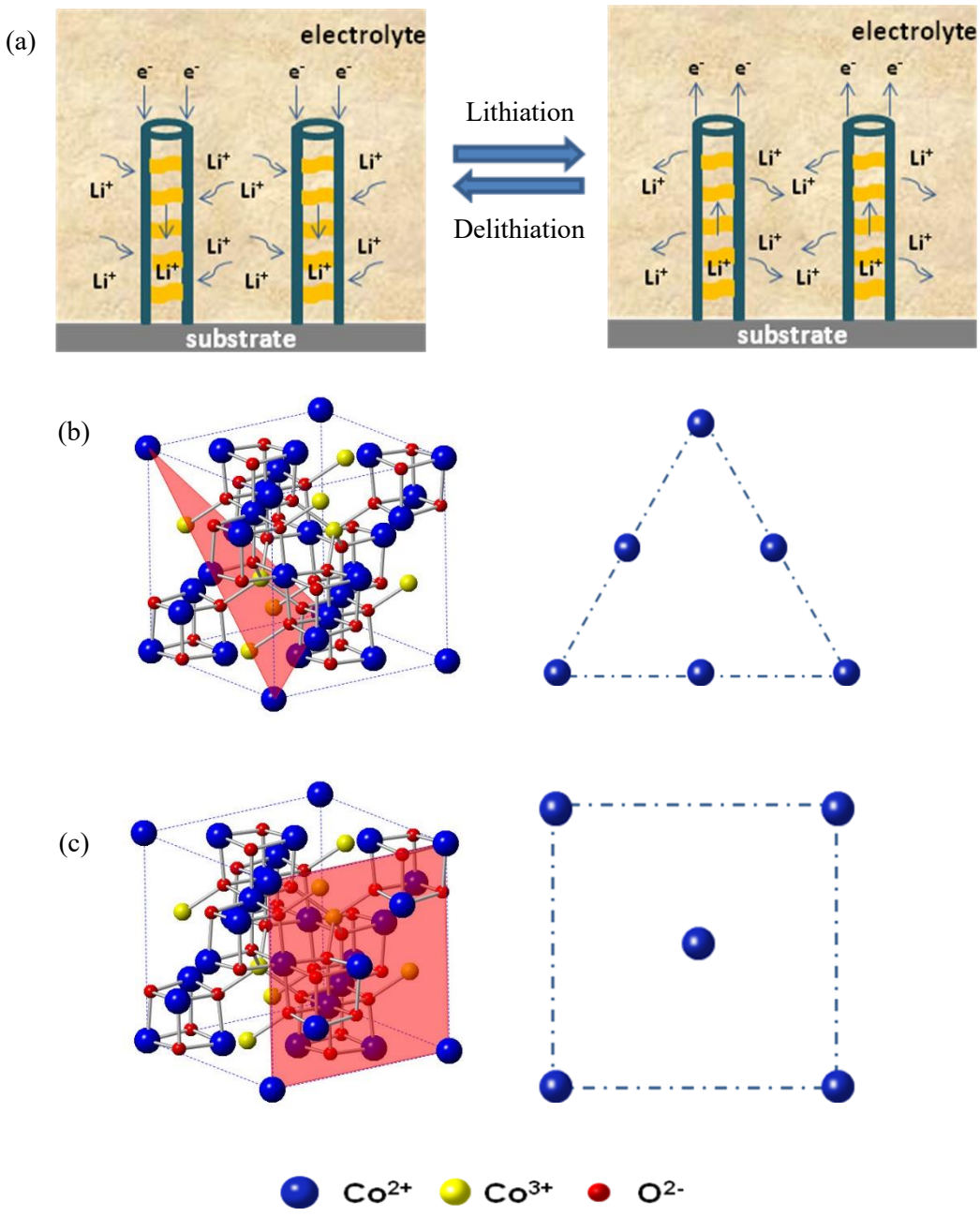


Fig. 8. (a) Schematic illustration of the Li ion insertion-extraction process for nanosheets-in-nanotube $Co_3O_4$/carbon arrays. (b) A theoretical model of 3D and 2D surface atomic configurations in the (111) plane of $Co_3O_4$. (c) A theoretical model of 3D and 2D surface atomic configurations in the (001) plane of $Co_3O_4$.

## 4. Conclusions

In summary, a new structure, nanosheets-in-nanotube $Co_3O_4$/carbon array, has been

successfully fabricated via a modified chemical vapor deposition method. As tested as anode materials for LIBs, as-prepared NIN structure showed the superior electrochemical performances, including excellent cycling life (850 mAh $g^{-1}$ after 200 cycles at 0.5C) and rate performance (694 mAh $g^{-1}$ at 2C). The real-time lithiation process and the atomic storage mechanisms of an NIN were further investigated by using an *in situ* TEM. During $Li^+$-uptake, a NIN structure could exhibit a good structural stability, resulting in its performance improvement.

**Declarations of interest: None**

**Acknowledgments**

This work was supported by "the Fundamental Research Funds for the Central Universities" (No. 2018JBZ107, No. 2018RC022, No. 2017JBM068, No. S18I00010, No. S17I00010), "the Natural Science Foundation of Inner Mongolia" [2017MS(LH)0205], and "the Research Program of Science and Technology at Universities of Inner Mongolia Autonomous Region" (NJZZ17081). The authors also appreciate the support from the "1000 Youth Talent plan" project and the "Excellent One Hundred" project of Beijing Jiaotong University. Y.Y. thanks the financially support by "the Fundamental Research Funds for the Central Universities" (No. 2017JBM068).

## References


[1] Z. Yang, J. Zhang, M. C. W. Kintner-Meyer, X. Lu, D. Choi, J. P. Lemmon, et al., Electrochemical energy storage for green grid, Chem. Rev. 111 (2011) 3577-3613.

[2] P. G. Bruce, B. Scrosati, J.-M. Tarascon, Nanomaterials for rechargeable lithium batteries, Angew. Chem. Int. Ed. 47 (2008) 2930-2946.

[3] K. Amine, I. Belharouak, Z. Chen, T. Tran, H. Yumoto, N. Ota, et al., Nanostructured anode material for high-power battery system in electric vehicles, Adv. Mater. 22 (2010**)** 3052-3057.

[4] J.-M. Tarascon, M. Armand, Issues and challenges facing rechargeable lithium batteries, Nature 414 (2001) 359-367.

[5] S. Ren, R. Prakash, D. Wang, V. S. K. Chakravadhanula, M. Fichtner, $Fe_3O_4$ anchored onto helical carbon nanofibers as high-performance anode in lithium-ion batteries, ChemSusChem 5 (2012) 1397-1400.

[6] T. Chen, Y. Hu, B. Cheng, R. Chen, H. Lv, L. Ma, et al., Multi-yolk-shell copper oxide@carbon octahedral as high-stability anodes for lithium-ion batteries, Nano Energy 20 (2016) 305-314.

[7] S.-Y. Lee, K.-Y. Park, W.-S. Kim, S. Yoon, S.-H. Hong, K. Kang, et al., Unveiling origin of additional capacity of $SnO_2$ anode in lithium-ion batteries by realistic *ex situ* TEM analysis, Nano Energy 19 (2016) 234-345.

[8] X. Zhu, Y. Zhu, S. Murali, M. D. Stoller, R. S. Ruoff, Nanostructured reduced graphene oxide/$Fe_2O_3$ composite as a high-performance anode material for lithium ion batteries, ACS Nano 5 (2011) 3333-3338.

[9] J. Li, Y. Hou, X. Gao, D. Guan, Y. Xie, J. Chen, et al., A three-dimensionally interconnected carbon nanotube/layered $MoS_2$ nanohybrid network for lithium ion battery anode with superior rate capacity and long-cycle-life, Nano Energy 16

(2015) 10-18.

[10] J. Zhou, J. Qin, X. Zhang, C. Shi, E. Liu, J. Li, et al., 2D space-confined synthesis of few-layer $MoS_2$ anchored on carbon nanosheet for lithium-ion battery anode, ACS Nano 9 (2015) 3837-3848.

[11] W.-J. Zhang, A review of the electrochemical performance of alloy anodes for lithium-ion batteries, J. Power Sources 196 (2011) 13-24.

[12] C. K. Chan, X. F. Zhang, Y. Cui, High capacity Li ion battery anodes using Ge nanowires, Nano lett. 8 (2008) 307-309.

[13] M. G. Kim, J. Cho, Nanocomposite of amorphous Ge and Sn nanoparticles as an anode material for Li secondary battery, J. Electrochem. Soc. 156(4) (2009) A277-A282.

[14] S. Yoon, C.-M. Park, H.-J. Sohn, Electrochemical characterizations of germanium and carbon-coated germanium composite anode for lithium-ion batteries, Electrochem. Solid-State Lett. 11(4) (2008) A42-A45.

[15] D. Ding, Y. Wang, X. Li, R. Qiang, P. Xu, W. Chu, et al., Rational design of core-shell Co@C microspheres for high-performance microwave absorption, Carbon 111 (2017) 722-732.

[16] Z. Chen, S. Wang, Z. Zhang, W. Zhou, D. Chen, Facile synthesis of $Co_3O_4$/Co@N-doped carbon nanotubes as anode with improved cycling stability for Li-ion batteries, Electrochim. Acta 292 (2018) 575-585.

[17] X. Deng, S. Zhu, F. He, E. Liu, C. He, C. Shi, et al., Three-dimensionally hierarchical $Co_3O_4$/carbon composites with high pseudocapacitance contribution for enhancing lithium storage, Electrochim. Acta 283 (2018) 1269-1276.

[18] X. Wu, Z. Han, X. Zheng, S. Yao, X. Yang, T. Zhai, Core-shell structured $Co_3O_4$@$NiCo_2O_4$ electrodes grown on flexible carbon fibers with superior

electrochemical properties, Nano Energy 31 (2017) 410-417.

[19] Y. Yang, X. Liu, Z. Dai, F. Yuan, Y. Bando, D. Golberg, et al., In situ electrochemistry of rechargeable battery materials: status report and perspectives, Adv. Mater. 29(31) (2017) 1606922.

[20] Z. Li, X.-Y. Yu, U. Paik, Facile preparation of porous $Co_3O_4$ nanosheets for high-performance lithium ion batteries and oxygen evolution reaction, J. Power Sources 310 (2016) 41-46.

[21] X. Wang, Q. Weng, Y. Yang, Y. Bando, D. Golberg, Hybrid two-dimensional materials in rechargeable battery applications and their microscopic mechanisms, Chem. Soc. Rev. 45 (2016) 4042-4073.

[22] A. M. M. Jani, D. Losic, N. H. Voelcker, Nanoporous anodic aluminium oxide: Advances in surface engineering and emerging applications, Prog. Mater. Sci. 58 (2013) 636-704.

[23] Y. Lin, H. Ji, Z. Shen, Q. Jia, D. Wang, Enhanced acetone sensing properties of $Co_3O_4$ nanosheets with highly exposed (111) planes, J. Mater. Sci.: Mater. Electron. 27 (2016) 2086-2095.

[24] D. Larcher, G. Sudant, J.-B. Leriche, Y. Chabre, J.-M. Tarascon, The electrochemical reduction of $Co_3O_4$ in a lithium cell, J. Electrochem. Soc. 149(3) (2002) A234-A241.

[25] Z.-S. Wu, W. Ren, L. Wen, L. Gao, J. Zhao, Z. Chen, et al., Graphene anchored with $Co_3O_4$ nanoparticles as anode of lithium ion batteries with enhanced reversible capacity and cyclic performance, ACS Nano 4 (2010) 3187-3194.

[26] D. Gu, W. Li, F. Wang, H. Bongard, B. Spliethoff, W. Schmidt, et al., Controllable synthesis of mesoporous peapod-like $Co_3O_4$@carbon nanotube arrays for high-performance lithium-ion batteries, Angew. Chem. Int. Ed. 54 (2015) 7060-7064.

[27] G. Huang, F. Zhang, X. Du, Y. Qin, D. Yin, L. Wang, Metal organic frameworks route to *in situ* insertion of multiwalled carbon nanotubes in $Co_3O_4$ polyhedra as anode materials for lithium-ion batteries, ACS Nano 9 (2015) 1592-1599.

[28] D. Wang, Y. Yu, H. He, J. Wang, W. Zhou, H. D. Abruña, Template-free synthesis of hollow-structured $Co_3O_4$ nanoparticles as high-performance anodes for lithium-ion batteries, ACS Nano 9 (2015) 1775-1781.

[29] Y. Hou, J. Li, Z. Wen, S. Cui, C. Yuan, J. Chen, $Co_3O_4$ nanoparticles embedded in nitrogen-doped porous carbon dodecahedrons with enhanced electrochemical properties for lithium storage and water splitting, Nano Energy 12 (2015) 1-8.

[30] Y. Chu, J. Feng, Y. Qian, S. Xiong, Enhancing the electrode performance of $Co_3O_4$ through $Co_3O_4$@a-$TiO_2$ core-shell microcubes with controllable pore size, RSC Adv. 5 (2015) 40899-40906.

[31] C. Li, T. Chen, W. Xu, X. Lou, L. Pan, Q. Chen, et al., Mesoporous nanostructured $Co_3O_4$ derived from MOF template: a high-performance anode material for lithium-ion batteries, J. Mater. Chem. A 3 (2015) 5585-5591.

[32] G.X. Pan, X.H. Xia, F. Cao, J. Chen, Y.J. Zhang, Construction of Co/$Co_3O_4$-C ternary core-branch arrays as enhanced anode materials for lithium ion batteries, J. Power Sources 293 (2015) 585-591.

[33] S. Qiu, H. Gu, G. Lu, J. Liu, X. Li, Y. Fu, et al., Rechargeable $Co_3O_4$ porous nanoflake carbon nanotube nanocomposite lithium-ion battery anodes with enhanced energy performances, RSC Adv. 5 (2015) 46509-46516.

[34] X. Wang, H. Guan, S. Chen, H. Li, T. Zhai, D. Tang, et al., Self-stacked $Co_3O_4$ nanosheets for high-performance lithium ion batteries, Chem. Commun. 47 (2011) 12280-12282.

[35] X. Wang, X.-L. Wu, Y.-G. Guo, Y. Zhong, X. Cao, Y. Ma, et al., Synthesis and lithium storage properties of $Co_3O_4$ nanosheet-assembled multishelled hollow spheres, Adv. Funct. Mater. 20 (2010) 1680-1686.

[36] J. Dong, Y. Xue, C. Zhang, Q. Weng, P. Dai, Y. Yang, et al., Improved $Li^+$ storage through homogeneous N-doping within highly branched tubular graphitic foam, Adv. Mater. 29(6) (2017) 1603692.

[37] D. A. Walters, L. M. Ericson, M. J. Casavant, J. Liu, D. T. Colbert, K. A. Smith, et al., Elastic strain of freely suspended single-wall carbon nanotube ropes, Appl. Phys. Lett. 74(25) (1999) 3803-3805.

[38] H. D. Wangner, O. Lourie, Y. Feldman, R. Tenne, Stress-induced fragmentation of multiwall carbon nanotubes in a polymer matrix, Appl. Phys. Lett. 72(2) (1998) 188-190.

[39] T. Belytschko, S. P. Xiao, G. C. Schatz, R. S. Ruoff, Atomistic simulations of nanotube fracture, Phys. Rev. B 65(23) (2002) 235430.

**Figure captions**

Fig. 1. (a) Schematic design and fabrication process of nanosheets-in-nanotube $Co_3O_4$/carbon arrays structure. (b) Schematic of the synthesis process of CNTs using the AAO template.

Fig. 2. (a) SEM image on the cross section of the broken nanosheets-in-nanotube $Co_3O_4$/carbon arrays structure. (b) HRTEM image of $Co_3O_4$ nanosheets from a side view.

Fig. 3. (a) XRD pattern of nanosheets-in-nanotube $Co_3O_4$/carbon arrays on the Cu foil. (b) SEM characterizations of nanosheets-in-nanotube $Co_3O_4$/carbon arrays. (c) TEM image at higher magnification of an individual nanosheets-in-nanotube $Co_3O_4$/carbon array structure. Inset showing the schematic drawing of nanosheets-in-nanotube $Co_3O_4$/carbon array. (d) HRTEM images of a nanosheets-in-nanotube $Co_3O_4$/carbon array layer.

Fig. 4. (a) Schematic of the fabrication process of the pure carbon nanotubes. (b) XRD pattern of carbon nanotubes. (c, d) SEM characterizations of carbon nanotubes. (e) HAADF STEM image and the EDS element mappings of C and O of carbon nanotubes. (f) HAADF STEM image of the nanosheets-in-nanotube $Co_3O_4$/carbon arrays structure. The EDS element mappings of O (g), Co (h) and C (j) of the nanosheets-in-nanotube $Co_3O_4$/carbon arrays structure.

Fig. 5. High-resolution XPS spectra of nanosheets-in-nanotube $Co_3O_4$/carbon arrays.

Fig. 6. Electrochemical lithium storage properties of nanosheets-in-nanotube $Co_3O_4$/carbon arrays: (a) Charge/discharge voltage profiles of nanosheets-in-nanotube $Co_3O_4$/carbon arrays at a current density of 0.2C. (b) Cycling performance and Coulombic efficiency of nanosheets-in-nanotube $Co_3O_4$/carbon arrays and commercial

$Co_3O_4$ at a current density of 0.2C. (c) Rate performance of nanosheets-in-nanotube $Co_3O_4$/carbon arrays at different current density. (d) EIS of nanosheets-in-nanotube $Co_3O_4$/carbon arrays and commercial $Co_3O_4$.

Fig. 7. (a) Schematic illustration of a LIB device with the anode of nanosheets-in-nanotube $Co_3O_4$/carbon arrays under *in situ* TEM. (b, c) *In situ* TEM patterns during Li ion intercalation and the FFT patterns of a nanosheets-in-nanotube $Co_3O_4$/carbon array. (d, e) TEM image at higher magnification of a nanosheets-in-nanotube $Co_3O_4$/carbon array. (f, g) HRTEM images of a nanosheets-in-nanotube $Co_3O_4$/carbon array layer before and after the Li ion intercalation. Inset showing the schematic drawing of the atomic structure.

Fig. 8. (a) Schematic illustration of the Li ion insertion-extraction process for nanosheets-in-nanotube $Co_3O_4$/carbon arrays. (b) A theoretical model of 3D and 2D surface atomic configurations in the (111) plane of $Co_3O_4$. (c) A theoretical model of 3D and 2D surface atomic configurations in the (001) plane of $Co_3O_4$.